Biomaterials 35 (2014) 8261–8272

Contents lists available at ScienceDirect

Biomaterials

journal homepage: www.elsevier.com/locate/biomaterials

A general strategy to achieve ultra-high gene transfection efficiency using lipid-nanoparticle composites

Raviraj Vankayala [a], Chi-Shiun Chiang [b], Jui-I. Chao [c], Chiun-Jye Yuan [c], Shyr-Yeu Lin [c, d, e], Kuo Chu Hwang [a, *]

[a] Department of Chemistry, National Tsing Hua University, Hsinchu 30013, Taiwan
[b] Department of Biomedical Engineering and Environmental Sciences, National Tsing Hua University, Hsinchu 30013, Taiwan
[c] Department of Biological Science, National Chiao Tung University, Hsinchu 30013, Taiwan
[d] Department of Biomedical Sciences, Chung Shan Medical University, Taichung, Taiwan
[e] Department of Obstetrics and Gynecology, Department of Medical Research, Stem Cell Lab, Mackay Memorial Hospital, Taipei 10449, Taiwan

ARTICLE INFO

Article history:
Received 2 June 2014
Accepted 6 June 2014
Available online 25 June 2014

Keywords:
Gene transfection
Gene therapy
Nanocarriers
Zebrafish
Cytotoxicity
Carbon nanoparticles

ABSTRACT

Gene therapy provides a new hope for previously "incurable" diseases. Low gene transfection efficiency, however, is the bottle-neck to the success of gene therapy. It is very challenging to develop non-viral nanocarriers to achieve ultra-high gene transfection efficiencies. Herein, we report a novel design of "tight binding-but-detachable" lipid-nanoparticle composite to achieve ultrahigh gene transfection efficiencies of 60~82%, approaching the best value (~90%) obtained using viral vectors. We show that Fe@CNPs nanoparticles coated with LP-2000 lipid molecules can be used as gene carriers to achieve ultra-high (60–80%) gene transfection efficiencies in HeLa, U-87MG, and TRAMP-C1 cells. In contrast, Fe@CNPs having surface-covalently bound N,N,N-trimethyl-N-2-methacryloxyethyl ammonium chloride (TMAEA) oligomers can only achieve low (23–28%) gene transfection efficiencies. Similarly ultrahigh gene transfection/expression was also observed in zebrafish model using lipid-coated Fe@CNPs as gene carriers. Evidences for tight binding and detachability of DNA from lipid-nanoparticle nanocarriers will be presented.

© 2014 Elsevier Ltd. All rights reserved.

1. Introduction

Among various therapeutic approaches, gene therapy is a very promising method for the treatment of many diseases that are previously considered incurable, such as, Parkinson disease, cystic fibrosis, as well as various kinds of cancers [1–4]. Most of the biomedical investigations and clinical treatments involving gene therapy are of limited success owing to their poor cellular uptake and limited gene transfection efficiencies. Hence, an effective delivery system is vital to successful gene delivery/therapy [5–7]. To this end, viral (e.g., adenovirus and retrovirus) and non-viral (e.g., polymers, nanoparticles and liposomes) vectors have been developed. Viral vectors provide very efficient gene delivery and transfection efficiencies (~90%). However, viral vectors have many serious drawbacks, including, immunogenicity, carcinogenicity, inflammation, limited DNA carrying capacity, difficult to prepare in large scale, and high cost [7,41]. Non-viral vectors are much safer than viral vectors, and have the advantages of simple/easy preparation, absence or negligible specific immune-response. However, the gene transfection efficiencies of non-viral vectors are far lower than viral vectors in general. Among non-viral vectors, liposomes, cationic polymers, such as poly (ethyleneimine) (PEI), poly (amidoamine) (PAMAM) based dendrimers were widely used as gene delivery vectors. For example, the PAMAM based polypeptide dendrimers can achieve ~33% GFP gene transfection efficiency in HeLa cells [8]. In the case of bone marrow cells, the gene transfection efficiencies are 20% and 35% for PEI and PAMAM nanocarriers, respectively [9]. The causes responsible for low gene transfection efficiencies (20~35%) in non-viral vector systems are still not clear, albeit, most of non-viral vectors are able to bind with DNAs very effectively. Recently, many new nanomaterials such as, carbon nanotubes [10–12], graphene [13], silica nanoparticles [14], quantum dots [15], gold nanoparticles [16], nanorods [17], etc. were reported to act as DNA cargoes for gene therapy applications. However, these nanomaterial-based non-viral vectors suffer from many problems,

* Corresponding author.
E-mail address: kchwang@mx.nthu.edu.tw (K.C. Hwang).

http://dx.doi.org/10.1016/j.biomaterials.2014.06.016
0142-9612/© 2014 Elsevier Ltd. All rights reserved.

such as, poor cellular uptake, inefficient gene release, high cytotoxicity and susceptible to intracellular degradation of foreign genes which results in poor transfection efficiencies. Although a variety of nanomaterials have been reported in the literature as nanocarriers for gene delivery and gene therapy with a wide range of gene transfection efficiencies, it remains very challenging to design a nanocarrier system to achieve ultra-high gene transfection efficiencies, similar to that obtained by viral vectors. The gene transfection efficiencies achieved upon using various non-viral vectors reported in the literature were summarized in Table 1. In general, many factors could possibly affect the gene transfection efficiencies, including, (a) high binding affinity between the nano-cargo and DNA polyplex, (b) high intracellular uptake of the DNA-nanocargoes [18], (c) efficient endosomal/lysosomal degradation of foreign DNA [19], and (d) poor DNA release from nanocarriers into the nucleus [18]. The factors (a) and (b) are favorable towards high gene transfection efficiency, but (c) and (d) are negative factors. Very high binding affinity between cationic nanocarriers and polyanionic DNA will favor carrying large quantity of genes, but it is un-favorable for efficient release of the gene being delivered [18]. Most of non-viral vectors reported in the literature to date emphasize efficient gene delivery via increasing the positive charges on nanocarriers), but still suffer from poor transfection efficiencies, presumably due to very poor gene release. If a nanocarrier can achieve both high gene binding affinity and high gene release efficiency simultaneously, high gene transfection efficiencies will be possible. To this end, we report a generalized approach in this paper to easily achieve ultra-high transfection efficiencies via a design of a nanocarrier system having tight binding affinity towards poly-anionic DNAs, but the neutral "DNA-lipid" complex is still detachable from the surface of nanocarriers.

Overall, we develop to prepare "tight binding-but-detachable" lipid-nanoparticle composites to achieve ultra-high gene transfection efficiencies in three different cell lines and as well as *in vivo* zebrafish model. Using our strategy, designing nanocarriers for efficient gene delivery/release for gene therapy treatments of various kinds of diseases can be easily explored in the clinical biomedicine.

2. Materials and methods

2.1. Synthesis of core/shell iron/carbon nanoparticles using solid state microwave arcing:

The magnetic core/shell iron encapsulated carbon nanoparticles were prepared by following the literature procedure [20–23]. In brief, a $C_{60/70}$ and ferrocene (1:1 wt ratio) powder mixture together with small pieces of silicon ($1 \times 1 \times 1 \sim 2 \times 2 \times 1$ mm^3 from a broken silicon wafer) was irradiated with microwave inside a focused microwave oven (2.45 GHz, Discover system, CEM Corporation, USA) under an argon atmosphere (1 atm) for 15 s. The microwave irradiation process was repeated twice to have more completely carbonization of the carbon-containing powder. Finally, the magnetic products were collected using an external magnet, and structure characterization was performed by using a transmission electron microscope (TEM, JEOL, JEM-2100F, 200 kV).

Table 1
Comparison of gene transfection efficiencies achieved using various non-viral vectors reported in the literature to that of "tight binding but detachable" lipid-Fe@CNPs.

Non-viral vector	Cell line	% Gene transfection efficiency	Reference
Dendrimer	Bone marrow cells	20	[8]
Poly (amidoamine)	Bone marrow cells	35	[9]
LP-2000	HeLa	27	[12]
Carbon nanotubes	HeLa	38	[12]
GO-PEI	HeLa	13	[13]
PEI-Silica nanoparticles	COS-7	44	[14]
Quantum dots	A549	40	[15]
Gold nanoparticles	Eukaryotic cells	25	[16]
Gold nanorods	HeLa cells	51	[17]
Gemini cationic lipids	HeLa cells	60	[45]
Lipid-Fe@CNPs	HeLa cells	78	Present study
Lipid-Fe@CNPs	U87-MG cells	80	Present study
Lipid-Fe@CNPs	TRAMP-C1	68	Present study

2.2. Surface functionalization of iron-encapsulated carbon nanoparticle (Fe@CNPs) [24,25]

To introduce fluorescent properties to Fe@CNPs, we modified the surface of the magnetic carbon soot. To the toluene solution (7 mL) containing magnetic carbon soot (50 mg) was added to the styrene monomer (1 mL, Aldrich) and benzoyl peroxide (BPO, 0.25 mL, 0.4 M) followed by ultrasonication (20 min) to make the carbon soot become well dispersed. The solution was transferred immediately to a domestic microwave oven (2.45 GHz, 600 W) and exposed to microwave irradiation for 10 s. During microwave irradiation the solution temperature rises rapidly, causing decomposition of the BPO radical initiator and initiation of polymerization. This addition of styrene-BPO-microwave irradiation process was repeated twice. The third time an additional component, namely, methacryloxy thiocarbomyl Rhodamine-B (MATCR, 10 mg in 1 mL THF), was added and the solution was sonicated and irradiated with microwaves under the same conditions. The fluorescent moiety, i.e., MATCR, was added to the Fe@CNPs-containing solution at a subsequent stage of surface grafting to avoid close contact with the graphene shells as photo-excited fluorescent moiety might be electronically quenched by the graphene shells on the Fe@CNPs surface. Finally, the surface-functionalized Fe@CNPs (designated as Fe@CNPs-PS-PMATCR) were collected and separated from free unbound polymers on repeated washing with THF and toluene and centrifugation at 12,000 rpm.

2.3. Synthesis of lipid-folate conjugates [25]:

In a typical experiment, 1:1 equivalents of 4-phenyl butyl amine and folic acid (Aldrich) were mixed with 1.1 equivalents of N,N'-Dicyclohexylcarbodiimide (DCC, Fluka) and dissolved in 15 mL dichloromethane (DCM) and stirred at room temperature for 24 h under nitrogen atmosphere. The resulting mixture was poured into a 5 wt% brine solution and undergone layer separation. The organic layer was washed and extracted for several times and final product was obtained by rotary evaporation of the residual solvent.

2.4. Preparation of lipid-Fe@CNPs

In empty round bottom flask, 50 μL of LP-2000 (Invitrogen, USA) and 50 μL of 5 wt% lipid-folate were spread over the bottom surface area and diluted with 300 μL of distilled water. To this solution, 1 mg of Fe@CNPs-PS-PMATCR was added and ultrasonicated for 5–10 min to get a homogenous dispersion. Then the mixture was further diluted with 600 μL distilled water to make up a volume until 1 mL and ultrasonicated again for another 5 min. Finally the lipid-to-nanoparticle weight ratio was maintained as 1:10. For the sake of clarity, the lipid-Fe@CNPs-PS-PMATCR will be designated as lipid-Fe@CNPs.

2.5. Preparation of DNA-lipid-Fe@CNPs and DNA-Fe@CNPs-TMAEA complexes

Different concentrations of DNA plasmids were diluted with PBS buffer and 10 μg of lipid-Fe@CNPs or Fe@CNPs-TMAEA were added and vortexed for 10 s and then incubated at 37 °C for 30 min to get stabilized. Then these complexes were further subjected to the cell line for the transfection assay experiments.

2.6. Surface modification of Fe@CNPs with N, N, N-trimethyl–N-(2-methacryloxyethyl) ammonium chloride

In a typical experiment, Fe@CNPs (50 mg) was suspended in an aqueous solution (8 mL) containing N,N,N-trimethyl–N-(2-methacryloxyethyl) ammonium chloride (TMAEA) (1 mL) monomer. The solution was then ultrasonicated in a bath-type ultrasonicator for 2 min to help disperse the core/shell iron/carbon nanoparticles. A tetrahydrofuran (THF) solution (0.25 mL) containing benzoyl peroxide (22.5 mg) was added to the solution, followed by ultrasonication for an additional 10 min. This process was repeated for 4 or 5 times with a total amount of 90–120 mg benzoyl peroxide added. The final solution was then diluted with deionized water, filtered through a nylon 66 (0.45 μm) membrane, and washed with deionized water several times to thoroughly remove free, unbound polymers [22].

2.7. In vitro magnetic resonance imaging (MRI) assays

MR images used in this study were acquired in a 7T MR imager (BioSpec 70/30 USR; Bruker). For T_2 measurements, lipid-Fe@CNPs and commercial Resovist agent (MagQu, Taiwan) with various concentrations of iron were dispersed in 0.5% agarose gel solution. The acquired MRIs and T_2 values were obtained using multislice multiecho sequence (MSME) with the following parameters, TR = 6000 ms; TE = 11~110 ms; matrix size = 256 × 256; field of view (FOV) = 60 × 60 mm^2; slice thickness = 6 mm. The total volume of each MRI phantom was 0.2 mL. Only 0.5% agarose gel solution was used as a control.

2.8. Zeta-potential and DLS measurements

The pDNA-lipid-Fe@CNPs complexes were prepared accordingly from the above mentioned procedures. The surface charge and average particle size was measured using Zeta-sizer instrument (Malvern, UK).

2.9. Estimation of binding constants using isothermal titration caloriemetry (ITC)

Isothermal titration caloriemetry experiments were carried out at 25 °C on a high precision ITC-200 (MicroCal, LLC, and Northampton, MA). The samples using different nanocarriers, such as, lipid-Fe@CNPs, LP-2000 and Fe@CNPs-TMAEA were prepared under the same conditions as adopted for transfection experiments. Before measurements, all the samples were degassed for at least 7 min before the titrations. ITC experiments were carried out in phosphate buffer solution at pH = 7.4. As a control set of experiments, buffer-to-buffer and buffer-to-DNA were also performed. The plasmid DNA was loaded into the cell and the nanocarrier was loaded into the syringe. 20 injections were performed with an each titration volume of 2 μL. The reference power of 5 μcal/s was applied while the sample contents were stirred at 400 rpm.

2.10. Synthesis of fluorescent lipid structures

In a typical experiment, 1:1 equivalents of 4-phenyl butyl amine and 9-anthracene carboxylic acid were dissolved in 20 mL dichloromethane solvent and to this N,N'-Dicyclohexylcarbodiimide and N-hydroxy succinimide were added. The reaction mixture was vigorously stirred for 24 h in the presence of nitrogen atmosphere. After 24 h, 5 wt% brine solution was added into the mixture in order to remove the by product, dicyclohexyl urea. The organic layer was extracted after several washings and distilled under rotary evaporator to collect the fluorescent lipid product.

2.11. Cell culture, materials and reagents

HeLa, U87MG and TRAMP-C1 cells were grown in Dulbecco's Minimum Essential Medium (DMEM, Gibco, and Grand Island, NY, USA) supplemented with 10% heat-inactivated fetal bovine serum (Invitrogen, Carlsbad, CA, USA), 2 mM L-glutamine, and 100 μg/mL penicillin and 100 U/mL streptomycin. The cells were grown in a humidified incubator at 37 °C (95% humidity, 5% CO_2). Other chemicals were purchased from Sigma Aldrich (St. Louis, MO, USA).

2.12. Transfection and cellular uptake assay

Transfection and cellular uptake was carried out procedures using as described elsewhere. HeLa, U87-MG and TRAMP-C1 were cultured in 6-well plates with Dulbecco's Modified Eagle's Medium (DMEM) (GIBCO, Invitrogen, Inc., Carlsbad, CA, USA) supplemented with 10% (v/v) Fetal Bovine Serum (FBS) at an initial density of 2×10^5 cells per well. It was 60% confluent on the day of transfection. After 24 h seeding, the cells were washed with phosphate buffer solution, and then 2 mL of the serum-free DMEM was added to each well. Finally, the cells were transfected with the DNA-lipid-Fe@CNPs or DNA-Fe@CNPs-TMAEA complexes. After 4 h incubation (duration of transfection) at 37 °C (under 5% CO_2), the medium was changed to DMEM supplemented with 10% FBS and further incubated for 48 h. After 48 h incubation the cells were washed with PBS buffer and trypsinized with 1 mL trypsin and centrifuged at 1000 rpm for 5 min. After repeating the washing process for two times, finally fix the cells with 1 mL of 0.1% p-formaldehyde/in PBS All experiments were repeated three times. Finally the cell suspensions were analyzed and 10,000 cells were collected using flow cell cytometry, in which the fluorescence from PE channel was attributed for the cellular uptake and the fluorescence from FITC channel was attributed for the transfection of GFP gene.

2.13. Confocal microscopy

HeLa cells (12.5×10^3 cells per well in 6-well plates) cultured in DMEM (Dulbecco's modified-eagle medium) supplemented with FBS (Fetal Bovine Serum, 10%) and penicillin-streptomycin (1%) were treated with DNA-lipid-Fe@CNPs or DNA-Fe@CNPs-TMAEA for 4 h. After 4 h, the cells were washed twice with phosphate buffer solution (PBS, pH 7.4) and then incubated for another 20 h. Then the cells were washed again with PBS, further fixed onto a glass slide using p-formaldehyde solution (4%) in PBS for 5 min, and washed with PBST (5% Tween-20 in PBS) solution three times; then Triton X-100 solution (1 mL) was added. After exposure to Triton X-100 (1 h), the HeLa cells were stained with DAPI (4′, 6-diamidino-2- phenylindole, 1 ng/mL PBS, 30 min). The samples were examined under a confocal laser-scanning microscope (OLYMPUS FV500) equipped with an InGaN semiconductor laser (405 nm), an Ar laser (488 nm), and a He–Ne laser (543 nm).

2.14. Preparation of DNA-lipid-nanomaterials complexes

In an empty round bottom flask, 50 μL of LP-2000 was spread over the bottom surface area and diluted with 300 μL of distilled water. To this solution, 1 mg of non-polar nanomaterial (NM) was added and ultrasonicated for 5–10 min to get a homogenous dispersion (carbon black (CB), magnetic nanodiamonds (MNDs) and reduced graphene oxide (RGO) are the three NM chosen in the present study). Then the mixture was further diluted with distilled water to make up a volume until 1 mL and ultrasonicated for another 5 min. The mixture was then filtered through 0.45 μm membrane filter to remove the large aggregates and then readily used for the complexation with plasmid DNA. Different concentrations of DNA plasmids were diluted with PBS buffer and certain aliquots of lipid-NM complexes were added and vortexed for 10 s and then incubated at 37 °C for 30 min to get stabilized. Then those complexes were further subjected to the cell line for the transfection assay experiments. For measuring the percentages of cellular uptake using flow cytometry with pDNA-lipid-CB complexes, 100 μg/mL of blue fluorescent lipid was added during the preparation of lipid-CB complexes.

2.15. Transfection and cellular uptake assay

Transfection and cellular uptake was carried out procedures using as described elsewhere. HeLa cells were cultured in 6-well plates with Dulbecco's Modified Eagle's Medium (DMEM) (GIBCO, Invitrogen, Inc., Carlsbad, CA, USA) supplemented with 10% (v/v) Fetal Bovine Serum (FBS) at an initial density of 2×10^5 cells per well. It was 60% confluent on the day of transfection. After 24 h seeding, the cells were washed with phosphate buffer solution, and then 2 mL of the serum-free DMEM was added to each well. Finally, the cells were transfected with the DNA-lipid-NM complexes. After 4 h incubation (duration of transfection) at 37 °C (under 5% CO_2), the medium was changed to DMEM supplemented with 10% FBS and further incubated for 48 h. After 48 h incubation the cells were washed with PBS buffer and trypsinized with 1 mL trypsin and centrifuged at 1000 rpm for 5 min and suspended in 1 mL PBS. Finally the cell suspensions were analyzed and 10,000 cells were collected using flow cell cytometry, in which the fluorescence from DAPI channel was attributed for the cellular uptake (for blue fluorescent lipid) and the fluorescence from FITC channel was attributed for the transfection of GFP gene.

2.16. Western blot analysis

Briefly, proteins were separated on 10~12% sodium dodecyl sulfate–polyacrylamide gels, and transferred electrophoretically onto polyvinylidene difluoride membranes. The membranes were sequentially hybridized with primary antibody and followed with a horseradish peroxidase-conjugated secondary antibody. Thereafter, the protein bands were visualized on the X-ray film using the enhanced chemiluminescence detection system (PerkinElmer Life and Analytical Sciences, Boston, MA). A gel-digitizing software, Un-Scan-It gel (ver. 5.1; Silk Scientific, Inc., Orem, UT) was used to quantify the relative intensity.

2.17. Gel retardation experiment

In a typical experiment, DNA was first mixed with the desired amount of lipid-Fe@CNPs or Fe@CNPs-TMAEA (DNA/NP = 0.9) in the PBS solution (pH ~ 7.4). After incubation at 37 °C for 15 min, the mixtures were loaded into a 0.8% agarose gel in tris–acetate–EDTA (TAE) buffer. The gel was allowed to run for 30 min at 150 V (7.5 v/cm) and then it was photographed under UV light.

2.18. Nuclease degradation experiment

In a typical experiment, DNA was first mixed with the desired amount of lipid-Fe@CNPs or Fe@CNPs-TMAEA (DNA/NP = 0.9). To test the extent of nuclease degradation ability, DNAse I (5 μg/mL) was added and incubated at 37 °C for 4 h, and then the mixtures were loaded into a 0.8% agarose gel in tris–acetate–EDTA (TAE) buffer. The gel was allowed to run for 30 min at 150 V (7.5 v/cm) and then it was photographed under UV light.

2.19. Annexin V apoptosis assay

HeLa and U87-MG cells were seeded into 6-well plates with the density of 200,000 cells per well. After 24 h, lipid-Fe@CNPs or Fe@CNPs-TMAEA stock solutions were added into cells and incubated for 1 h. Cells were then trypsinized, aspirated and suspended in 2 mL PBS. Cells were further stained with PE-Annexin-V (5 μL) and 7-AAD (5 μL) from the BD Annexin-V apoptosis kit and then keep it stand by for 15 min at room temperature in darkness, followed by flow cytometry analysis.

2.20. Reactive oxygen species (ROS) generation

HeLa and U87-MG cells were seeded into 6-well plates with the density of 200,000 cells per well. After 24 h, lipid-Fe@CNPs or Fe@CNPs-TMAEA stock solutions were added into cells and incubated for 4 h. Cell Culture medium was replaced with 2, 7-dichlorofluorescien diacetate (DCFH-DA) solution (5 μM in cell culture medium) and incubated with cells for 30 min at 37 °C. Cells were then trypsinized and aspirated, followed by flow cytometry analysis. Green fluorescence was monitored.

2.21. Cytotoxicity assay

One milliliter of HeLa cell-containing solution (~2.12×10^3 cells/mL) was added to each well of a 24-well plate and incubated 1 day to allow cells to stick on the surface of the plate. Aliquots of a PBS buffer solution containing different amounts of DNA with 10 μg of lipid-Fe@CNPs or Fe@CNPs-TMAEA were added to the 24-well plate, and the cell solutions were incubated for another 3 days. A 50 μL amount of an MTT aqueous solution (0.5 mg/mL) was added to each well of the 24-well plate 4 h before termination of the 3-days incubation, and the cells were allowed to

incubate for another 4 h. Then, the upper layer of the solutions in the 24-well plate was discarded, and 1 mL of DMSO was added to each well to lyse cell membrane followed by pipette stirring. The final solution in each well was centrifuged at 13,000 rpm to remove any solid residues before measurements of the optical absorbance at 570 nm. The optical absorbances were converted to cell viabilities based on a standard curve (absorbance vs cell numbers) obtained from controlled experiments carried out under the same condition except that no nanoparticles were added during cell culture processes.

2.22. Incubation of lipid-Fe@CNPs conjugates under ATP depletion

For the ATP depletion studies, the cells were pre-incubated in PBS buffer solution and supplemented with 10 mM sodium azide for 30 min at 37 °C followed by incubation in a solution of DNA-lipid-Fe@CNPs conjugates.

2.23. Folic acid pre-treatment for blocking folate receptors

To estimate the entry of nanoparticles via receptor mediated endocytosis, the cells were pre-incubated in 1 mM folic acid in complete medium for 30 min at 37 °C followed by incubation in a solution of DNA-lipid-Fe@CNPs conjugates.

2.24. Microinjection of DNA-lipid-Fe@CNPs or DNA-Fe@CNPs-TMAEA into zebrafish embryos

Wild-type AB strains of Danio rerio (zebrafish) embryos obtained from zebrafish core facility center, National Tsing Hua University were used in all the experiments. Fresh embryos were collected on to the microinjection embryo tray just before the experiment. DNA-Lipid-Fe@CNPs or DNA-Fe@CNPs-TMAEA or naked DNA were diluted at appropriate concentrations in double distilled water and sonicated up until microinjection. Approximately 10 nL volume was microinjected into the animal pole region of embryos between stages 1 (one cell embryo) and 3 (four cell embryo) using Drummond microinjector. Each experiment was performed on 50 embryos per condition. Following microinjection, embryos were transferred onto the petri dish filled with the system water and incubated at 28 °C in dark condition. For the *in vivo* cytotoxicity measurements, the live embryos were counted each day until 72 hpf (hours post fertilization). After the 72 hpf, all the developed embryos were hatched manually and examined the types of abnormalities undergone through fluorescence microscope (Nikon, E600). For *in vivo* imaging experiments, the zebrafish embryos (72 hpf) were hatched and fixed on the cover slips (15 × 16 mm, GeneFrame) with 1% agarose gel (Sigma, USA) to monitor the fluorescence of lipid-Fe@CNPs using CLSM (10x, LSM-700, Zeiss).

3. Results and discussion

3.1. Preparation and characterization of Fe@CNPs

The water dispersible, magnetic and fluorescent Fe@CNPs was prepared by following a sonication-microwave irradiation surface functionalization process (Fig. S1) [26]. After the surface functionalization process, the structure of Fe@CNPs was examined under transmission electron microscopy (TEM) and reveals a well-graphitized graphene shells with an iron nanoparticle core in the center (Fig. S2(a)). The fluorescent properties of Fe@CNPs-PS were evaluated in Fig. S2(b) and reveals an emission maximum at 572 nm. The magnetization curve in Fig. S2(c) shows that Fe@CNPs-PS exhibit super paramagnetic behavior with a saturation magnetization value of 23 emu/g and their effectiveness as magnetic resonance imaging contrast reagents were also determined (see Fig. S2(d) and (e)). The amounts of surface functionalities grafted on the surface of Fe@CNPs were quantified using thermograviemetric analyses (TGA) and the surface functional groups were confirmed using FT-IR analyses (see Figs. S3 and S4) [26]. The red fluorescent Fe@CNPs were further mixed with Lipofectamine 2000 (LP-2000) along with 5 wt% lipid-folate (see Fig. S5) and sonicated for 10 min to form lipid-Fe@CNPs hybridized structures (see supporting information for more details).

3.2. In vitro cellular uptake, gene transfection and cytotoxicity

In general, positively charged gene delivery vectors can effectively form complexes with poly-anionic DNA via electrostatic attraction. Hence, the zeta-potentials for lipid-Fe@CNPs, Fe@CNPs-TMAEA and LP-2000 liposomes were measured in the presence of serum and serum-free conditions (Fig. S6). In the presence of serum-free medium, they exhibit highly positive charge, but turn to negatively charged in the presence of serum. It was well known that the serum proteins can adsorb onto the cell membrane and influence the surface charge of the non-viral vectors [27]. After complexation with pDNA, both lipid-Fe@CNPs and Fe@CNPs-TMAEA exhibit an average particle sizes ranging from 120~150 nm and the surface charge becomes negative as the pDNA concentration was increased (Fig. S7). The plasmid used in this study is GFP-encoded circularly coiled DNA of molecular weight ~4.5 kbp (see Fig. S8). During the transfection process, DNA might be degraded, due to the lack of protection, by the intracellular nucleases, leading to poor gene transfection efficiencies. To examine whether complexation of polyanionic pDNA with cationic lipid-Fe@CNPs and Fe@CNPs-TMAEA can result in (partial) protection of pDNA from being degraded by nuclease, nuclease degradation experiments were performed. The results shown in Fig. S9 clearly reveal that free naked DNA was completely degraded, whereas complexation of pDNA with nanocarriers indeed can have some extents of protection from nuclease degradation. The percentages of pDNA being degraded are 40% and 60%, for pDNA-lipid-Fe@CNPs and pDNA-Fe@CNPs-TMAEA, respectively. The pDNA molecules in complex forms do not have the same molecular conformation as that of free DNA, and thus do not fit with the nuclease active site, leading to protection from degradation. The protection effect from lipid-Fe@CNPs is better than that for Fe@CNPs-TMAEA. Overall, the DNA protection ability for different nanocarriers is in the following order: lipid-Fe@CNPs > Fe@CNPs-TMAEA > naked DNA.

In order to evaluate the cellular uptake and gene transfection efficiencies using both types of gene delivery vectors, HeLa cells were pretreated with pDNA-lipid-Fe@CNPs and pDNA-Fe@CNPs-TMAEA for 4 h. After 4 h uptake, pDNA-nanoparticle complexes were washed away and the cells were allowed to have 20 h incubation before GFP fluorescence measurements. The fluorescence property of surface-functionalized Fe@CNPs allows one to track the exact location of the nanoparticles using confocal laser scanning microscopy (CLSM). Fig. 1(a) shows that most of the nanoparticles were distributed in the cytoplasm regime in which the Fe@CNPs red fluorescence was overlapped with the green fluorescent proteins (GFP) expression for both the types of nanocarriers, lipid-Fe@CNPs and Fe@CNPs-TMAEA. The extent of GFP fluorescence was far more intense for lipid-Fe@CNPs as compared to the Fe@CNPs-TMAEA system. To determine the exact percentages of cellular uptake and gene transfection efficiency simultaneously, HeLa cells were fed with both pDNA-lipid-Fe@CNPs and pDNA-Fe@CNPs-TMAEA with different DNA-to-nanocarrier charge ratios for 4 h. The current Fe@CNPs has surface-grafted red fluorescent moieties, i.e., methacryloxy thiocarbomyl Rhodamine-B (MATCR), which allows one to measure the percentage of cellular uptake by flow cell cytometry. A series of experiments were performed by varying the DNA-to-nanocarrier charge ratio. The efficacy of GFP expression and cellular uptake were evaluated for 10^5 cells using flow cytometry. The cellular uptake percentages for both the type of delivery vectors were about 60–80%, at higher DNA-to-nanocarrier charge ratios in HeLa and U-87MG cell lines (see Fig. 1(b)). To check whether similar cellular uptake can be achieved for the 'difficult to transfect' cells, TRAMP-C1 cells were also fed with both types of nanocarriers for 4 h uptake. As expected from the results in HeLa cells, TRAMP-C1 cells also exhibit a high percentage of cellular uptake (~70%) when lipid-Fe@CNPs was used as a carrier, whereas only 50% uptake was observed with the Fe@CNPs-TMAEA nanocarrier. The gene transfection efficiencies for both the nanocarriers in all three cell lines, namely, HeLa, U-87MG and "difficult-to-transfect" TRAMP-C1 cell lines, were plotted in Fig. 1(c) as a

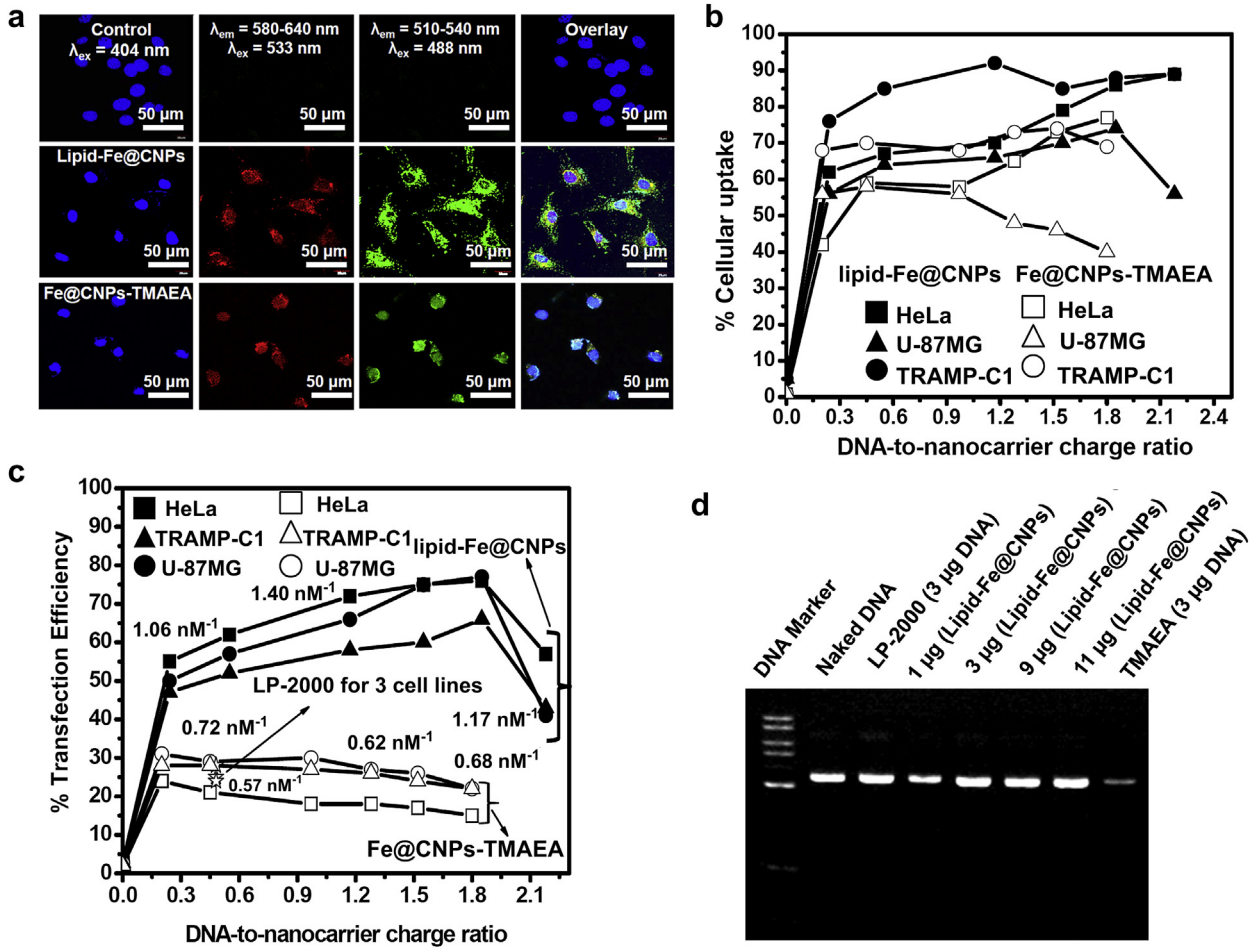

Fig. 1. Intracellular uptake and gene delivery in different cells (a) Confocal laser scanning optical images of HeLa cells at 20 h after internalized with lipid-Fe@CNPs and Fe@CNPs-TMAEA, respectively. The DNA-to-nanocarrier charge ratio is 1.8 for both lipid-Fe@CNPs and Fe@CNPs-TMAEA. The green fluorescence was from GFP and the red fluorescence from the Fe@CNPs and nucleus was stained with DAPI dye. (b) Cellular uptake of different nanocarriers was monitored using flow cytometry for all the three cell lines. (c) Gene transfection efficiencies monitored using flow cytometry in HeLa, U-87MG and TRAMP-C1, respectively, by different nanocarriers. Binding constant between the respective nanocarrier and DNA was expressed in nanomolar (nM^{-1}) concentration range, and labeled in the plot. (d) Gel retardation assay to determine the amounts of DNA being released from different gene delivery vectors-DNAs complexes. The amount of naked DNA used in the experiment was 3 μg.

function of DNA-to-nanocarrier charge ratio. With the increase in the DNA-to-nanocarrier charge ratio, the gene transfection efficiency was increased and reached a plateau value of 65–78% using lipid-Fe@CNPs as a gene carrier, which is ~2.2 fold higher than the gene transfection efficiencies (24–27%) using the widely used LP-2000 liposomes as gene carrier in all the three cell lines. On contrary, when Fe@CNPs-TMAEA was used as a delivery vector, very poor gene transfection efficiencies (23–28%) were achieved, despite of similar cellular uptake efficiencies as that of lipid-Fe@CNPs. The poor gene transfection efficiencies of 23–28% were attributed to the poor DNA release from the surface of Fe@CNPs-TMAEA nanocarriers (vide infra). The best gene transfection efficiency of 68% using the lipid-Fe@CNPs nanocarrier is 3.4 times higher than that using LP-2000 (20%, see Fig. 1(c), and is also 1.7 times of the best gene transfection efficiency (40%) ever reported in the literature for this notoriously "difficult-to-transfect" TRAMP-C1 cells [28]. To understand the causes responsible for the ultrahigh gene transfection efficiencies using the lipid-Fe@CNPs nanocarriers, we further determine the binding constants between different nanocarriers and plasmid DNA. The binding constants for different nanocarriers at different DNA-to-nanocarrier charge ratios were measured using isothermal titration calorimetry (ITC) (see Fig. S10) and binding constants labeled in the Fig. 1(c). The lipid-Fe@CNPs exhibits stronger binding affinities to plasmid DNA than Fe@CNPs-TMAEA and LP-2000 under the same DNA-to-nanocarrier charge ratio (see Fig. 1(c)). The larger the binding constants, the more DNA will be delivered, possibly leading to higher gene transfection efficiencies. At extremely high binding constant, no gene release is possible. At extreme low binding constant, no delivery of gene is possible. Both the cases will result in very low gene transfection efficiencies. Therefore, compromising the binding affinity (with a medium-to-high binding constant) and gene release efficiency will give the best gene transfection. Such a behavior can qualitatively explain the bell shape gene transfection efficiencies patterns observed in both the lipid-Fe@CNPs and the Fe@CNPs-TMAEA nanocarriers systems (see Fig. 1(c)). At a given DNA-to-nanocarrier charge ratio, increasing the binding constant will enable a nanocarrier to carry more amount of plasmid DNA per nanocarrier. To be able to carry more amount of plasmid DNA will certainly favor higher gene transfection efficiency, if the accompanied larger binding constant does not result in a poor gene release. How can it be possible that a larger binding constant does not result in a poor gene release? Yes, this will be possible if polyanionic DNAs remain tightly bound with cationic surface moieties on nanocarriers while the whole neutral "pDNA-surface moieties" complex can detach from the surface of nanocarriers inside cells.

This is exactly the case here for the "detachable" lipid-Fe@CNPs where plasmid DNA forms tight binding complex with the surface coating cationic lipid molecules. The "DNA-lipid" complex can detach from the surface of Fe@CNPs inside cells, which is not possible for the Fe@CNPs-TMAEA nanocarrier system, since the TMAEA moieties were chemically linked onto Fe@CNPs. Therefore, the lipid-Fe@CNPs nanocarrier system not only can carry more amount of plasmid DNA (by a larger binding constants), but also is able to release cargoes more efficiently than the Fe@CNPs-TMAEA nanocarrier system. Overall, the lipid-Fe@CNPs nanocarrier always shows much higher gene transfection efficiencies than the non-detachable Fe@CNPs-TMAEA nanocarrier system under the same DNA-to-nanocarrier charge ratios. The dissociation of DNA from the surface of nanocarriers can possibly proceed through two different pathways: (a) dissociation of polyanionic pDNA from nanocarrier surface via charge replacements/complexation with intracellular charged species, and (b) dissociation of the whole neutral "pDNA-lipid" complex from the surface of nanocarriers. In the pathway (a), intracellular metal cations, such as Ca^{2+}, Zn^{2+}, etc may form complexes with surface-bound polyanionic pDNA via strong electrostatic interactions, and facilitates DNA release from the surface of nanocarriers. Alternatively, anionic lipids present in the intracellular environment, such as phosphatidylserine (PS), may replace anionic DNA and form complexes with positive charges on nanocarriers. Upon the surface bound lipoplexes interact with the inner endosomal leaflet, this could induce the formation of transient pores or sites for membrane destabilization, which would create a way for DNA to detach from the nanocarrier and release to the cytosol [29,30]. In the pathway (b), the neutral "pDNA-lipid" complex might interact with the inner endosomal leaflet or membrane, and detach from the nonpolar Fe@CNPs surface. The pathway (b) is possible only for the lipid-Fe@CNPs nanocarrier, but not for the Fe@CNPs-TMAEA nanocarriers, where the cationic TMAEA moieties were chemically linked onto the Fe@CNPs nanocarrier (see Scheme 1). Overall, the lipid-Fe@CNPs nanocarrier has an additional DNA release pathway (b) than the tight bound, non-detachable Fe@CNPs-TMAEA nanocarrier, and thus has much higher gene transfection efficiencies.

The amount of GFP proteins expressed can also be detected by Western blot measurement (see Fig. S11), which is consistent with the percentages of gene transfection efficiencies shown in Fig. 1(c). In the case of LP-2000 liposome, DNA-lipid complex is also possibly detachable, the same as that in the lipid-Fe@CNPs nanocarrier system. However, LP-2000 liposome only utilizes half of its cationic surface charge, i.e., the outside surface layer, to bind with polyanionic DNA, and thus is much less efficient to deliver DNAs, as compared to the lipid-Fe@CNPs nanocarrier. In addition, the smaller binding constants of LP2000 toward polyanionic DNA at the same DNA-to-nanocarrier charge ratio also makes itself less efficient to deliver DNA than the lipid-Fe@CNPs nanocarrier. Consequently, LP-2000 liposome always has far lower (~2.2 times less) gene transfection efficiencies than those in the detachable lipid-Fe@CNPs nanocarrier system.

The ability of the "anionic DNA-cationic lipid" complex to detach from the surface of Fe@CNPs nanocarrier is evidenced by two experimental observations, namely, (a) gel retardation assay for DNA release; and (b) confocal fluorescent lipid measurements (vide infra). The much more efficient gene release from the DNA-lipid-Fe@CNPs complexes than other DNA-nanocarrier complexes is also supported by direct measurements of the amount of DNA released using an agarose gel electrophoresis (see Fig. 1(d)). From Fig. 1(d), we can observe that almost 75% of the surface bound DNA was released from the lipid-Fe@CNPs nanoparticle, whereas poly-cationic tight binding Fe@CNPs-TMAEA nanoparticles can only release 25% of surface bound DNA, and subsequently very poor gene transfection efficiencies were observed. The extent of DNA release from the carriers after internalization is very important in the transfection process [31]. It has been frequently observed poor gene transfection efficiency from poly-cationic nanocarriers [32], which provide tight binding with DNAs, and possibly poor release

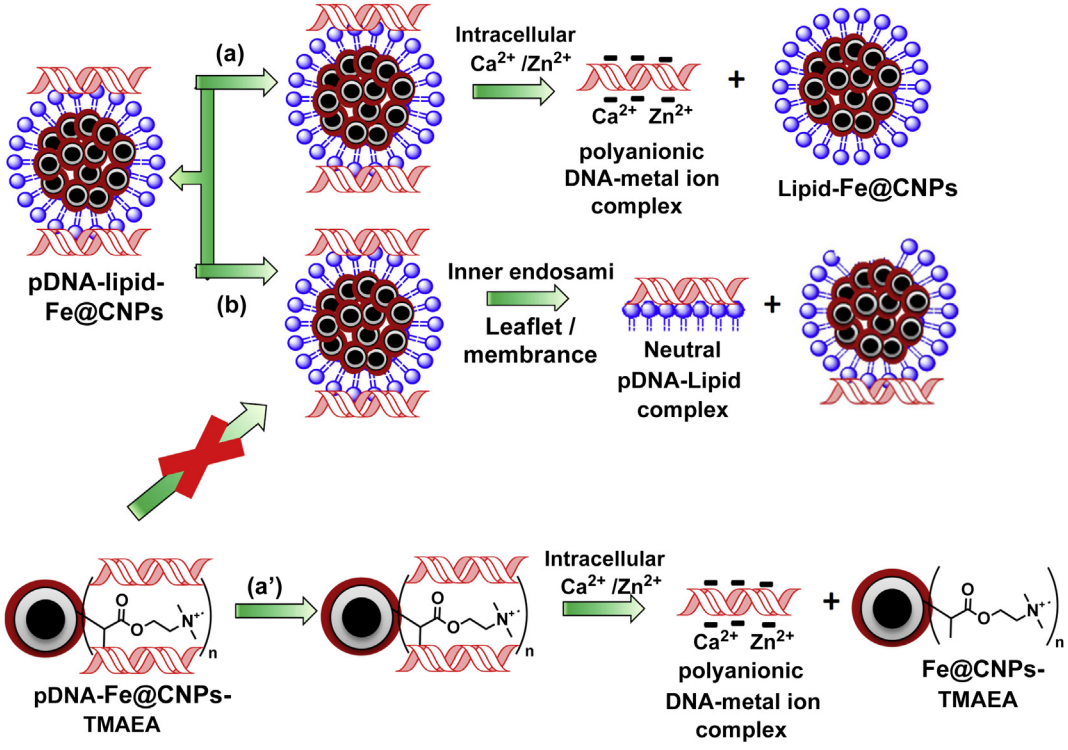

Scheme 1. Schematic representation for the dissociation of DNA from different nanocarriers, pDNA-lipid-Fe@CNPs and pDNA-Fe@CNPs-TMAEA, respectively.

of DNA. In this study, we illustrate that to have high efficiency of gene transfection, it is necessary to have very good detachability of the plasmid from the nanocarrier. Overall, our gel electrophoresis data support the idea that combination of tight binding as well as detachability between the nanocarrier and DNA is the key factor controlling ultra-high gene transfection efficiency. Based on these above findings, it clearly indicates that poor gene transfection reported in the literature using poly-cationic polymer beads is most probably due to the poor release ability of DNA from nano-carrier vectors, especially in the case of PEI [34] and PAMAM dendrimer-based vectors [8]. Even though it was reported that lower charge density of poly (amine-co-ester) terpolymers boosts the gene transfection efficiency (for example, ~2 orders for HEK293 cells) as compared to PEI and LP-2000 [33], it was never realized that "tight binding but detachable" is the key factor leading to high gene transfection efficiencies. Overall, the results in Fig. 1 demonstrate that "tight binding but detachable" nanocarriers can facilitate ultra-high gene expression, whereas tight binding/non-detachable nanocarriers results in poor gene transfection efficiency.

Using lipid-Fe@CNPs over LP-2000 as a gene carrier has the following advantages, (a) lipid-Fe@CNPs can facilitate the formation of nano-micelles with size ~150 nm (see Fig. S7 (a)), whereas LP-2000 might result in the formation of large liposomes of size ~930 nm (data not shown), which causes more interference to the cellular membrane structures; (b) In the case of lipid-Fe@CNPs all cationic lipid molecules can form electrostatic complexes with poly-anionic DNA, whereas only ~50% of lipid can form complexes with DNA in LP-2000 liposomes; (c) higher IC_{50} values for lipid-Fe@CNPs than LP-2000 in three cancer cell lines; (d) 3–4 fold high gene transfection efficiencies for lipid-Fe@CNPs than LP-2000 liposomes. In order to exclude the effect of serum proteins on the gene transfection efficiencies in both the nanocarrier systems, the intrinsic gene transfection efficiencies (by normalizing the observed gene transfection efficiency to the percentage of cellular uptake; so that cellular uptake factor can be excluded from the gene transfection efficiencies) were compared in the presence and absence of 10% fetal bovine serum (FBS). In the literature, it is well-known that the serum proteins can bind to the cellular membranes and thereby can hinder the percentages of cellular uptake as well as transfection efficiencies [46]. From Fig. S12 (a) and (b), it clearly shows that lipid-Fe@CNPs has superior gene transfection efficiencies inside the cells to that of Fe@CNPs-TMAEA system in all the three cell lines. In addition, similar intrinsic gene transfection efficiencies were obtained in both the nanocarriers irrespective of the presence or absence of serum (see Fig. S12(c)).

An additional advantage for lipid-Fe@CNPs hybridized nanostructures might be its lower cytotoxicity as compared with LP-2000 and carbon nanoparticles functionalized with TMAEA. From Fig. 2 (a), (b) and (c), the cytotoxicity levels for LP-2000 were said to be 0.1 μg/mL (IC_{50}) for HeLa and U87-MG, and 1.2 μg/mL (IC_{50}) for the TRAMP cell line, respectively. For lipid-Fe@CNPs, the IC_{50} value is 50 μg/mL for HeLa and 25 μg/mL for U87-MG as well as TRAMP, respectively. For Fe@CNPs-TMAEA, slightly higher levels of cytotoxicity than lipid-Fe@CNPs were observed in all the three cell lines. It was worthy to note that the cytotoxicity of LP-2000 was mainly caused by the direct electrostatic fusion of the cationic lipid

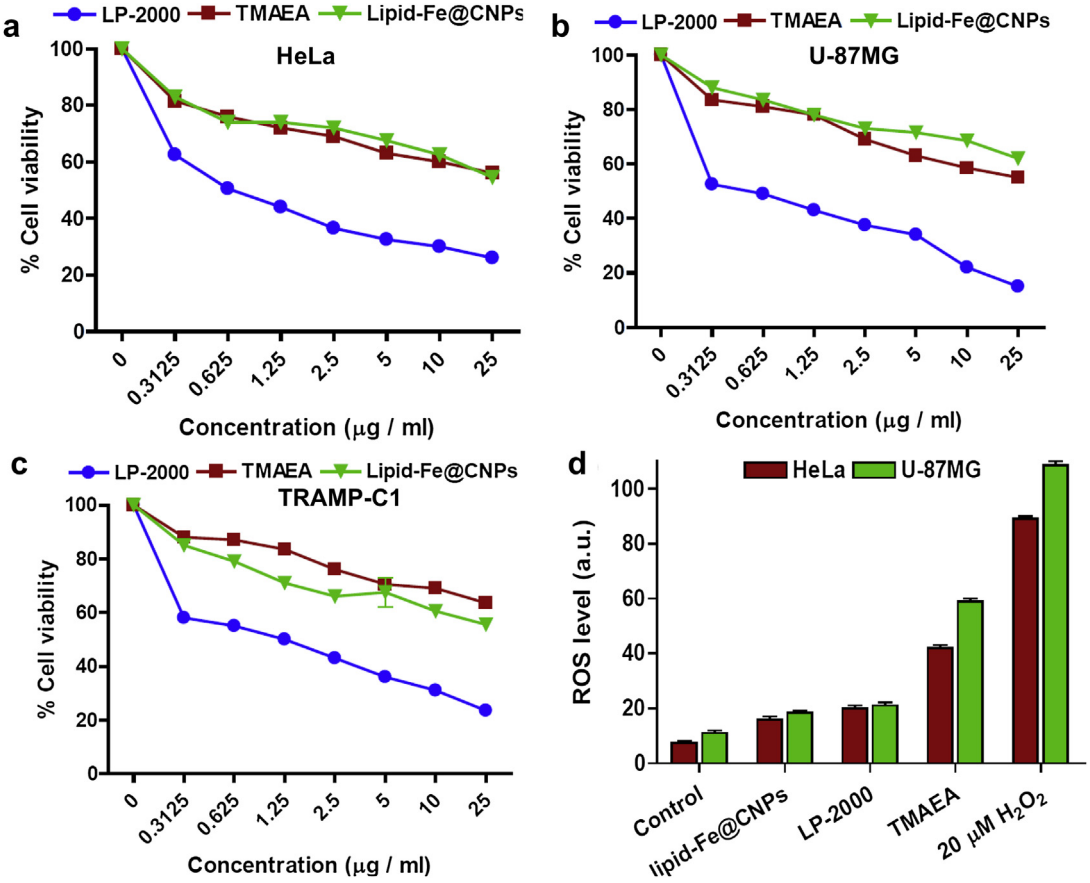

Fig. 2. Biocompatibility of lipid-Fe@CNPs, Fe@CNPs-TMAEA and LP-2000 (a), (b), and (c) represents the MTT cell viabilities monitored in HeLa, U-87MG and TRAMP-C1 cell lines, respectively. (d) Reactive oxygen species (ROS) generation monitored for all the nanoparticles fed to the HeLa cells for 24 h and the mean fluorescence intensities of DCF were quantified.

to the negatively charged cell membrane which causes rapid cell membrane destruction [32]. To compare the induction of oxidative stress by LP-2000, lipid-Fe@CNPs and Fe@CNPs-TMAEA, we monitored intracellular ROS generation by flow cytometry using a reductive reagent, 2′,7′−dichlorofluorescein (DCF). From Fig. 2(d), it shows that the ROS levels are comparable for lipid-Fe@CNPs and LP-2000, whereas Fe@CNPs-TMAEA has induced a much higher level of ROS.

3.3. *In vivo* fluorescence tracking, gene expression and cytotoxicity

In order to monitor the *in vivo* fluorescence tracking and gene expression with different nanocarriers, zebrafish was chosen as a model, owing to its high body transparency, similarity to mammals such as, mouse, rat and humans as well as its very easy maintenance [35]. From Fig. 3(a), the fluorescence microscopy images clearly reveal the levels of GFP gene expression in zebrafish using different nanocarriers. It was clearly evident that the GFP level for the lipid-Fe@CNPs system is ~300% higher than those from the free naked DNA, LP-2000, and the Fe@CNPs-TMAEA systems (see Fig. 3(b)). It is also interesting to note that, in the case of lipid-Fe@CNPs-DNA complex, the GFP gene expression has occurred selectively at the blood vessels to a greater extent as compared to the other organs such as yolk-sac, head, and tail (see Fig. 4(a)). To figure out the reasons for the effective pDNA release and gene expression, we hypothesize that the neutral pDNA-lipid complex was effectively dissociated from the Fe@CNPs nanoparticle surface. To this end, we prepare non-polar blue fluorescent molecule (see supplementary Fig. S13) and then mix with the LP-2000. The confocal images in Fig. 4(b) clearly reveal that both *in vitro* as well as in the *in vivo* zebrafish model, the location of blue fluorescent lipid (i.e., blue fluorescence) was totally different from the location of red fluorescent Fe@CNPs, indicating that pDNA-lipid complexes were able to detach from the Fe@CNPs surface and thereby pDNA was transfected effectively. The gene expression in blood vessels and the distribution of nanoparticles were visualized by the *z*-axis confocal images (see Fig. S14). These images clearly show that the locations of red fluorescent Fe@CNPs, blue fluorescent lipid molecules, and expressed GFP in a zebrafish are very different, suggesting a very efficient release of the neutral pDNA-lipid complex from Fe@CNPs surface, whereas for Fe@CNPs-TMAEA, poor expression and tight overlap between red fluorescent Fe@CNPs-TMAEA and green GFP was observed (see Fig. 4(c)). The relatively much weaker GFP fluorescence and good overlap between GFP and the red fluorescence from the Fe@CNPs-TMAEA were observed, indicating that the pDNA was poorly released from the Fe@CNPs-

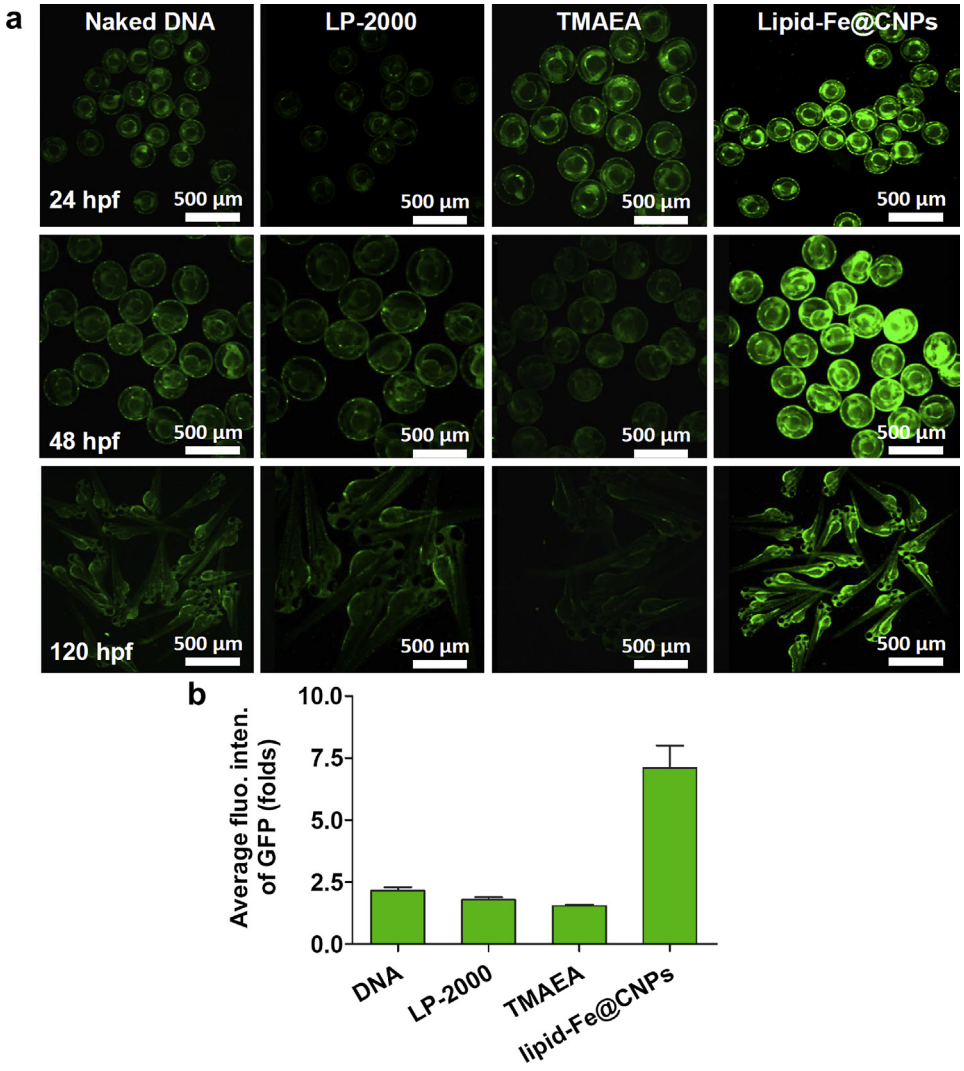

Fig. 3. *In vivo* gene expression in zebrafish after microinjection of different gene delivery vectors (a) Fluorescence microscopic images recorded at 5× magnification at different hpf to monitor the levels of GFP gene expression. (b) Average fluorescence intensity of GFP expression with different vectors monitored at 120 hpf.

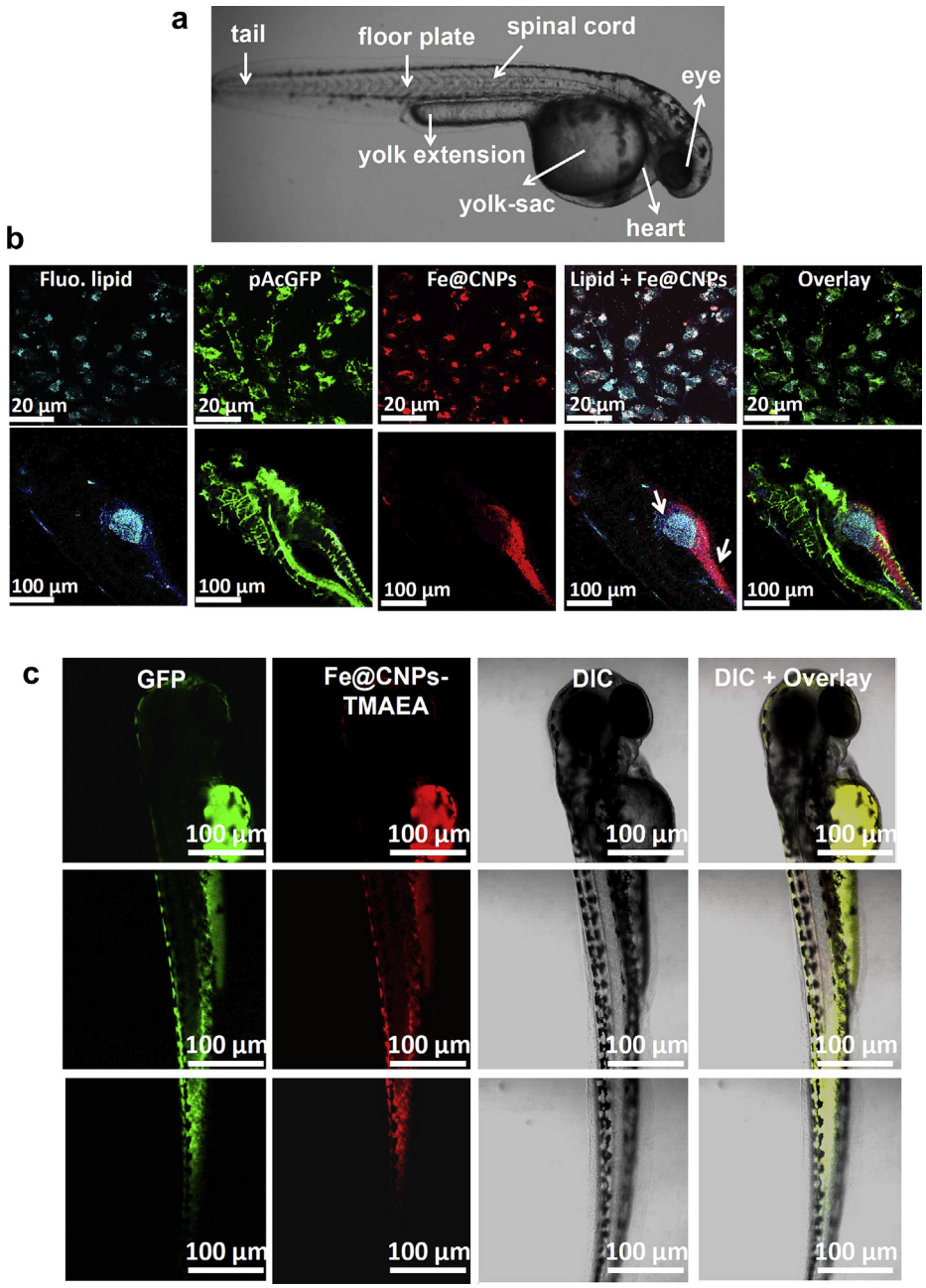

Fig. 4. (a) Optical image of a zebrafish under normal development at 72 hpf. (b) *In vitro* and *In vivo* gene expression using detachable pDNA-lipid-Fe@CNPs by confocal laser scanning optical microscopy. The images were recorded at 10× magnification for 72 hpf. The blue fluorescence was observed from lipid (λ_{ex} = 400 nm, λ_{em} = 410–440 nm), green fluorescence from GFP (λ_{ex} = 488 nm, λ_{em} = 505–540 nm) gene expression and the red fluorescence (λ_{ex} = 533 nm, λ_{em} = 570–630 nm) was derived from the fluorescent lipid-Fe@CNPs. The white arrow indicates the release of lipid-pDNA from the Fe@CNPs.

TMAEA nanocarriers (see Fig. 4(c)) and Fig. S15). In addition, the DNA release from the lipid-Fe@CNPs and GFP gene expression at different hours post fertilization (hpf) can also be visualized by confocal microscopy (see Fig. S16). Overall, both *in vitro* and *in vivo* gene expression results strongly support that DNA release or detachability from the nanocarrier is the key factor responsible for ultra-high gene transfection, whereas non-detachability or restriction in the DNA release down-regulates the transgene expression in the *in vitro* and *in vivo* zebrafish model system.

To study the *in vivo* cytotoxicities of free naked DNA, lipid-Fe@CNPs-DNA and Fe@CNPs-TMAEA-DNA complexes in the embryonic development of zebrafish, different doses of nanocargoes were microinjected into the 8-cell stage of the embryos. As the dosage of nano DNA cargoes increases, the number of normally developed zebrafish decreases, while the number of dead zebrafish increases (see Fig. 5(a)). The percentages of abnormalities induced after microinjection of different nanocarriers are summarized in Fig. 5(b). The results in Fig. 5(c) show that intact set of embryos did not show any abnormalities and the growth development is normal. Most of the free naked DNA microinjected embryos have induced yolk-sac abnormalities. At low doses of lipid-Fe@CNPs-DNA and Fe@CNPs-TMAEA-DNA complexes, the percentage of normally developed zebrafish is higher than that of the dead and deformed zebrafish. Cardiac malformation and yolk-sac edema were the most frequently observed abnormalities in zebrafish treated with both nanocarriers. Control experiments were done by

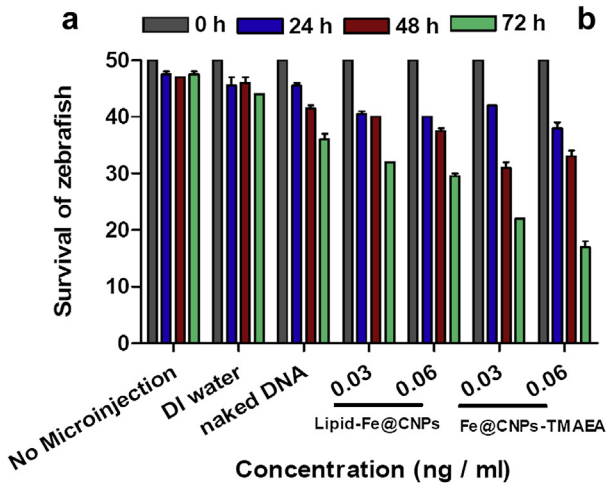

b

Summary for the mutations in zebra fish after microinjection of different gene delivery vectors (Total embryos =50)

Sample	Yolk sec Edema	Head Edema	Cardiac Malfunction	Eye Abnormality	Tail Flexure and Truncation
No microinjection	–	–	–	–	–
Naked DNA	+ (6%)	–	–	–	+ (4%)
Lipid-Fe@CNPs	+ (3%)	+ (4%)	–	–	+ (6%)
Fe@CNPs-TMAEA	–	+ (2%)	+ (11%)	–	+ (8%)

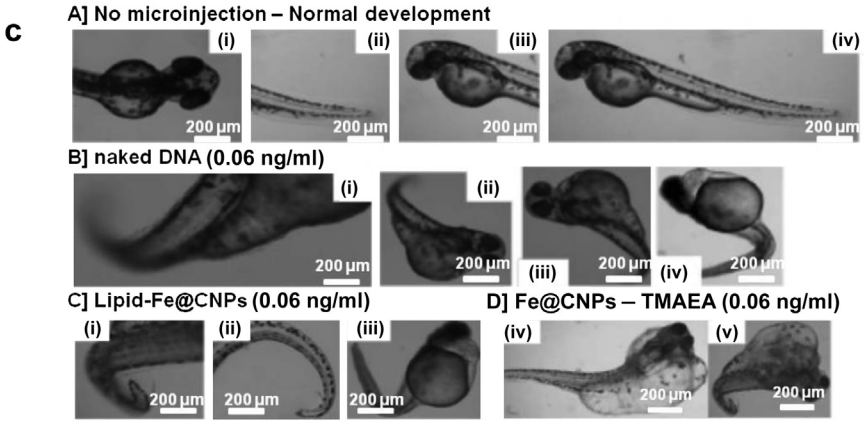

Fig. 5. Biocompatibility of different gene delivery vectors in zebrafish. (a) Survival rate of zebrafish after microinjection of gene delivery vectors such as, free naked DNA, lipid-Fe@CNPs and Fe@CNPs-TMAEA, respectively at different hours post fertilization (hpf). (b) Summary of the abnormalities in zebrafish induced after microinjection of different vectors. (c) Optical microscopic images of zebrafish for different abnormalities observed such as yolk-sac edema, head edema, eye abnormality, cardiac malfunction and tail truncation at 72 hpf.

microinjection of DI water and a set of embryos without microinjection to compare the survival rate of zebrafish under the same experimental conditions. The observed malformations and abnormalities in this study are also similar to that observed in zebrafish treated with Ag NPs [36,37], iron oxide NPs [38], dichloroacetic acid (DCA) [39] and cadmium [40]. Taken together, these results suggest that lipid-Fe@CNPs as nano DNA cargoes were considered to be very promising with low cytotoxicity in both *in vitro* and *in vivo* systems. Tight binding-but-detachability of the DNA-lipid complex is the key factor responsible for the observed ultra-high gene transfection efficiencies, whereas non-detachability restricts the release of DNA and also induces high cytotoxicity. These nanoparticles have also enabled us to track their location once it has been administered to the tumor cells or zebrafish model system. Overall, well protected and stable lipid-Fe@CNPs hybridized nanostructures was shown to be the most robust nanocarriers with tight binding, detachability, lower cytotoxicity, and ultra-high cellular uptake/gene transfection in both *in vitro* and *in vivo* which was not reported in any previous literature papers.

In principle, any non-polar nanomaterials, such as, polymer nanoparticles, metal nanoparticles, graphene nanoplates, etc, can be able to serve as nano-template and allow the cationic lipid molecules to form a surface coating layer. It is not necessary to be restricted to Fe@CNPs. To examine whether the above argument/strategy is generally applicable, we have replaced Fe@CNPs with the commercially available carbon black (CB) (preliminary particle size ~ 16 nm) and prepared the lipid-CB composite with different ratios. The average particle size was measured using DLS for different ratios of lipid-CB (see Fig. S19 (a)). Further, the cellular uptake and gene transfection efficiencies of pDNA-lipid-CB complexes (CB/lipid ratio ~ 66) were measured by using flow cytometry in the HeLa cells by varying the concentration of DNA. As shown in Fig. S19 (b), as the DNA concentration increases, the gene transfection efficiency was also increased and reached to a plateau value of 82%. In a similar way, we also achieved good gene transfection efficiencies (60–70%) for lipid-reduced graphene oxide (RGO) and lipid-magnetic nanodiamonds (MNDs) DNA complexes in HeLa cells (see Fig. S20). Overall, we have developed a simple and generalized strategy of lipid-nanoparticle composites with tight binding and easy detachability to achieve ultra-high gene transfection efficiencies.

We compare the transfection efficiencies and cytotoxicities of the available viral and non-viral synthetic DNA carrier systems in the literature to that of the lipid-Fe@CNPs (see Fig. 6) [41,42]. For example, adenoviral vectors can achieve a very high gene transfection efficiency of ~90%, but its acute cytotoxicity (80–90%), especially in causing viral infections, severely limits its clinical usage. Low-voltage electroporation can also improve naked DNA expression substantially (25–65%), however, its clinical use has been hampered as the low voltage short electrical pulses can cause trauma, and also is difficult or not applicable in in-vivo system for bulk scale gene therapy treatments. In addition, Gemini cationic

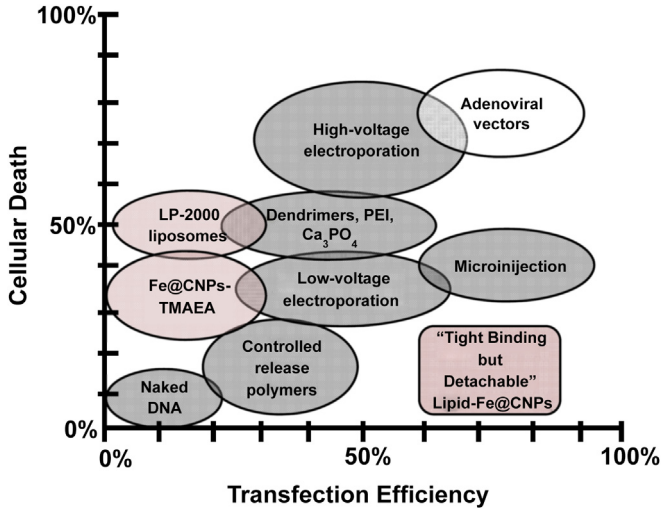

Fig. 6. Comparison of transfection efficiency versus cellular deaths for various DNA vectors with lipid-Fe@CNPs [41].

lipids were also reported to achieve high gene transfection efficiencies (50–70%) under serum-free conditions. The reasons to obtain high transfection efficiencies are totally unclear. Moreover, higher cytotoxicity of the Gemini cationic lipids severely limits its practical applicability [43–46]. Overall, it is very clear that the current "tight binding-but-detachable" lipid-Fe@CNPs system stands in a much better position with transfection efficiencies ranging from 60~80% and low cytotoxicities (<25% cellular deaths). In addition, the lipid-nanoparticle strategy can also be generalized, in which any non-polar nanomaterial can be readily coated with the cationic lipid molecules. Notice that the size and shape of nanomaterials in lipid-nanoparticle composites can also play a minor role affecting the gene transfection efficiencies [47,48], which have to be further optimized. Nevertheless, we have clearly demonstrated a general strategy that lipid-nanoparticle composites can work as highly efficient nano gene-carriers, of which the gene transfection efficiencies are approaching to viral vectors (~90%) with various nanomaterials.

4. Conclusions

We have reported a new strategy to design "tight binding-but-detachable" lipid-nanoparticle" nanocarriers to achieve ultra-high gene transfection efficiencies of 60~80%, approaching to the best values (~90%) from viral vectors, yet the cytotoxicity (<25%) is still far lower than viral vectors. The unique "tight binding-but-detachable" nanocarrier system is composed of a cationic lipid surface coating layer on non-polar nanocarriers, which not only is able to bind polyanionic pDNA tightly, provide partial protection of pDNA from degradation by intracellular nuclease, but is also able to detach from the surface of nanocarriers. Ultra-high transfection efficiencies of 78, 80 and 68% were obtained in HeLa, U-87MG and TRAMP-C1 cell lines, respectively, using "tightly bound but detachable" lipid-nanoparticle hybridized nanostructures. The gene transfection efficiencies from the "tightly binding-but-detachable" lipid-Fe@CNPs is 3~4 times higher than those (23~28%, and 24~27%, respectively) of tight binding/non-detachable Fe@CNPs-TMAEA and the most commonly used LP-2000 liposomes both *in vitro* and *in vivo*. In the *in vivo* zebrafish model, the "tight binding-but-detachable" nanocarrier also exhibits efficient and selective gene expression at the blood vessels, whereas naked DNA and Fe@CNPs-TMAEA showed poor gene expression and random distribution of GFPs. Overall, our results have pointed out a clear cut way for designing highly efficient nanocarriers for gene transfection, and in the future, this simple lipid-nanoparticle composite strategy will find wide biomedical applications to improve the efficiencies of gene transfection/gene therapy/gene silencing in treatments of various kinds of diseases.

Acknowledgments

The authors are grateful to the financial support from the Frontier Research Center on Fundamental and Applied Sciences of Matters, National Tsing Hua University and Ministry of Science and Technology, Taiwan (NSC 100-2113-M-007-007-MY3).

Appendix A. Supplementary data

Supplementary data related to this article can be found at http://dx.doi.org/10.1016/j.biomaterials.2014.06.016.

References

[1] Zhang J, Lei Y, Dhaliwal A, Ng QKT, Du J, Yan M, et al. Protein–polymer nanoparticles for nonviral gene delivery. Biomacromolecules 2011;12:1006–14.
[2] Lee SK, Tung C-H. A fabricated sirna nanoparticle for ultralong gene silencing in vivo. Adv Func Mater 2013;23:3488–93.
[3] Kelkar SS, Reineke TM. Theranostics: combining imaging and therapy. Bioconjug Chem 2011;22:1879–903.
[4] Lee JE, Lee N, Kim T, Kim J, Hyeon T. Multifunctional mesoporous silica nanocomposite nanoparticles for theranostic applications. Acc Chem Res 2011;44:893–902.
[5] Coune PG, Schneider BL, Aebischer P. Parkinson's disease: gene therapies. Cold Spring Harb Perspectives Med 2012;2:1–15.
[6] Griesenbach U, Geddes DM, Alton EWFW. Gene therapy for cystic fibrosis: an example for lung gene therapy. Gene Ther 2004;11:S43–50.
[7] Cuddington BP, Dyer AL, Workenhe ST, Mossman KL. Oncolytic bovine herpesvirus type 1 infects and kills breast tumor cells and breast cancer-initiating cells irrespective of tumor subtype. Cancer Gene Ther 2013;20:282–9.
[8] Wu HM, Pan SR, Chen MW, Wu Y, Wang C, Wen YT, et al. A serum-resistant polyamidoamine-based polypeptide dendrimer for gene transfection. Biomaterials 2011;32:1619–34.
[9] Peng L, Liu M, Xue Y-N, Huang S-W, Zhuo R-X. Transfection and intracellular trafficking characteristics for poly(amidoamine)s with pendant primary amine in the delivery of plasmid DNA to bone marrow stromal cells. Biomaterials 2009;30:5825–33.
[10] Wu Y, Phillips JA, Liu H, Yang R, Tan W. Carbon nanotubes protect dna strands during cellular delivery. ACS Nano 2008;2:2023–8.
[11] Herrero MA, Toma FM, Al-Jamal KT, Kostarelos K, Bianco A, Da Ros T, et al. Synthesis and characterization of a carbon nanotube–dendron series for efficient sirna delivery. J Am Chem Soc 2009;131:9843–8.
[12] Qin W, Yang K, Tang H, Tan L, Xie Q, Ma M, et al. Improved GFP gene transfection mediated by polyamidoamine dendrimer-functionalized multi-walled carbon nanotubes with high biocompatibility. Colloids Surf B: Biointerfaces 2011;84:206–13.
[13] Feng L, Zhang S, Liu Z. Graphene based gene transfection. Nanoscale 2011;3:1252–7.
[14] He W-T, Xue Y-N, Peng N, Liu W-M, Zhuo R-X, Huang S-W. One-pot preparation of polyethylenimine-silica nanoparticles as serum-resistant gene delivery vectors: intracellular trafficking and transfection. J Math Chem 2011;21:10496–503.
[15] Li Y, Duan X, Jing L, Yang C, Qiao R, Gao M. Quantum dot-antisense oligonucleotide conjugates for multifunctional gene transfection, mRNA regulation, and tracking of biological processes. Biomaterials 2011;32:1923–31.
[16] Crew E, Rahman S, Razzak-Jaffar A, Mott D, Kamundi M, Yu G, et al. Micro RNA conjugated gold nanoparticles and cell transfection. Anal Chem 2011;84:26–9.
[17] Chen C-C, Lin Y-P, Wang C-W, Tzeng H-C, Wu C-H, Chen Y-C, et al. DNA–gold nanorod conjugates for remote control of localized gene expression by near infrared irradiation. J Am Chem Soc 2006;128:3709–15.
[18] Cho SK, Kwon YJ. Polyamine/DNA polyplexes with acid-degradable polymeric shell as structurally and functionally virus-mimicking nonviral vectors. J Control Release 2011;150:287–97.
[19] Pinto-Gonzalez Howell D, Krieser RJ, Eastman A, Barry MA. Deoxyribonuclease II is a lysosomal barrier to transfection. Mol Ther 2003;8:957–63.
[20] Hsin Y-L, Lin C-F, Liang Y-C, Hwang KC, Horng J-C, Ho J-aA, et al. Microwave arcing induced formation and growth mechanisms of core/shell metal/carbon nanoparticles in organic solutions. Adv Func Mater 2008;18:2048–56.

[21] Liang Y-C, Hwang KC, Lo S-C. Solid-state microwave-arcing-induced formation and surface functionalization of core/shell metal/carbon nanoparticles. Small 2008;4:405–9.
[22] Mu Q, Yang L, Davis JC, Vankayala R, Hwang KC, Zhao J, et al. Biocompatibility of polymer grafted core/shell iron/carbon nanoparticles. Biomaterials 2010;31:5083–90.
[23] Hwang KC. Recent progress in the preparation and application of carbon nanocapsules. J Phys D Appl Phys 2010;43:374001.
[24] Hsin Y-L, Lai J-Y, Hwang KC, Lo S-C, Chen F-R, Kai JJ. Rapid surface functionalization of iron-filled multi-walled carbon nanotubes. Carbon 2006;44:3328–35.
[25] Hwang KC, Lai PD, Chiang C-S, Wang P-J, Yuan C-J. Neutron capture nuclei-containing carbon nanoparticles for destruction of cancer cells. Biomaterials 2010;31:8419–25.
[26] Chang IP, Hwang KC, Ho J-aA, Lin C-C, Hwu RJR, Horng J-C. Facile surface functionalization of nanodiamonds. Langmuir 2009;26:3685–9.
[27] Verma A, Stellacci F. Effect of surface properties on nanoparticle–cell interactions. Small 2010;6:12–21.
[28] Zuhorn IS, Hoekstra D. On the mechanism of cationic amphiphile-mediated transfection. To fuse or not to fuse: is that the question? J Membr Biol 2002;189:167–79.
[29] Kalderon D, Roberts BL, Richardson WD, Smith AE. A short amino acid sequence able to specify nuclear location. Cell 1984;39:499–509.
[30] Huang V, Place RF, Portnoy V, Wang J, Qi Z, Jia Z, et al. Upregulation of cyclin B1 by miRNA and its implications in cancer. Nucleic Acids Res 2011;12:13–21.
[31] Truong NP, Jia Z, Burgess M, Payne L, McMillan NAJ, Monteiro MJ. Self-catalyzed degradable cationic polymer for release of DNA. Biomacromolecules 2011;12:3540–8.
[32] Lainé C, Mornet E, Lemiègre L, Montier T, Cammas-Marion S, Neveu C, et al. Folate-equipped pegylated archaeal lipid derivatives: synthesis and transfection properties. Chem Eur J 2008;14:8330–40.
[33] Zhou J, Liu J, Cheng CJ, Patel TR, Weller CE, Piepmeier JM, et al. Biodegradable poly(amine-co-ester) terpolymers for targeted gene delivery. Nat Mater 2012;11:82–90.
[34] Thomas M, Klibanov AM. Conjugation to gold nanoparticles enhances polyethylenimine's transfer of plasmid DNA into mammalian cells. Proc Nat Acad Sci 2003;100:9138–43.
[35] Ko S-K, Chen X, Yoon J, Shin I. Zebrafish as a good vertebrate model for molecular imaging using fluorescent probes. Chem Soc Rev 2011;40:2120–30.
[36] Lee KJ, Nallathamby PD, Browning LM, Osgood CJ, Xu X-HN. In vivo imaging of transport and biocompatibility of single silver nanoparticles in early development of zebrafish embryos. ACS Nano 2007;1:133–43.
[37] Bowman CR, Bailey FC, Elrod-Erickson M, Neigh AM, Otter RR. Effects of silver nanoparticles on zebrafish (Danio rerio) and Escherichia coli (ATCC 25922): a comparison of toxicity based on total surface area versus mass concentration of particles in a model eukaryotic and prokaryotic system. Environ Toxicol Chem 2012;31:1793–800.
[38] Zhu X, Tian S, Cai Z. Toxicity assessment of iron oxide nanoparticles in zebrafish *danio rerio* early life stages. PLoS ONE 2012;7:e46286.
[39] Williams FE, Sickelbaugh TJ, Hassoun E. Modulation by ellagic acid of DCA-induced developmental toxicity in the zebrafish (Danio rerio). J Biochem Mol Toxicol 2006;20:183–90.
[40] Hallare AV, Schirling M, Luckenbach T, Köhler HR, Triebskorn R. Combined effects of temperature and cadmium on developmental parameters and biomarker responses in zebrafish (*Danio rerio*) embryos. J Therm Biol 2005;30:7–17.
[41] Luo D, Saltzman WM. Synthetic DNA delivery systems. Nat Biotechnol 2000;18:33–7.
[42] Djurovic S, Iversen N, Jeansson S, Hoover F, Christensen G. Comparison of nonviral transfection and adeno-associated viral transduction on cardiomyocytes. Mol Biotechnol 2004;28:21–31.
[43] Ryhänen SJ, Säily MJ, Paukku T, Borocci S, Mancini G, Holopainen JM, et al. Surface charge density determines the efficiency of cationic gemini surfactant based lipofection. Biophys J 2003;84:578–87.
[44] Zhao Y-N, Qureshi F, Zhang S-B, Cui S-H, Wang B, Chen H-Y, et al. Novel gemini cationic lipids with carbamate groups for gene delivery. J Mater Chem B 2014;2:2920–8.
[45] Muñoz-Úbeda M, Misra SK, Barrán-Berdón AL, Datta S, Aicart-Ramos C, Castro-Hartmann P, et al. How does the spacer length of cationic gemini lipids influence the lipoplex formation with plasmid DNA? Physicochemical and Biochemical Characterizations and their Relevance in Gene Therapy. Biomacromolecules 2012;13:3926–37.
[46] Misra SK, Biswas J, Kondaiah P, Bhattacharya S. Gene transfection in high serum levels: case studies with new cholesterol based cationic gemini lipids. PLoS ONE 2013;8:e68305.
[47] Cho EC, Au L, Zhang Q, Xia Y. The effects of size, shape, and surface functional group of gold nanostructures on their adsorption and internalization by cells. Small 2010;6:517–22.
[48] Zhang Y, Tekobo S, Tu Y, Zhou Q, Jin X, Dergunov SA, et al. Permission to enter cell by shape: nanodisk vs nanosphere. ACS Appl Mater Interfaces 2012;4:4099–105.